Solar Energy
and Sustainable Development
Refereed, biannual scientific journal issued by
The Libyan Center for Solar Energy Research and Studies

Thermochemical and Electrochemical Modeling Using MATLAB for Performance Evaluation of Low Temperature Electrolysers

Ibrahim H. Tawil[1*], Zahra Gebrel[2], Salem Matouq Khamkhem[3], Abdulnasir. S. Amir[4], Abdulhamid Salim Alajmi[5].

[1] Libyan Center for Solar Energy Research and Studies, Tajura, Libya.
[2] Faculty of Science, Sabrath University, Sabrath, Libya.
[3] Waha Oil Company, National Oil Corporation, Tripoli, Libya.
[4]Faculty of Natural Resources Engineering, Zawia University, Al-Ajailat, Libya.
[5]Faculty of Science Alsabiah Gharyan University, Gharyan, Libya

E-*mail:* [1*] ibrahim.h.tawil@csers.ly, [2]Zahra.gebrel@sabu.edu.ly, [3]salemmatouq@loey.org.ly, [4]a.salehamer@zu.edu.ly, [5]abdulhamidalajmi77@gmail.com

ARTICLE INFO.

Article history:
Received 16 September 2025
Received in revised 25 July 2026
Accepted 29 July 2026
Available online 01 August 2026

KEYWORDS

Water electrolysis, low operating temperature, hydrogen production, electrochemical, thermochemical.

ABSTRACT

This study presents a MATLAB-based computational model for the thermochemical and electrochemical analysis of low-temperature technologies. The model accurately predicts thermodynamic limits and key performance indicators, including reversible cell voltage and hydrogen production, as a function of operating temperature. Findings consistently demonstrate that increasing temperature reduces the reversible cell potential and Gibbs free energy change (ΔG), As a result, it lowers the electrical energy consumption for water splitting and improves the rate of hydrogen production. This analysis has validated that operating the Electrolyser at higher temperatures results in consistently higher performing AEM (50-80C), AWE (60-90C), and PEM (50-100C) systems by lowering cell voltage, boosting the amount of hydrogen produced per minute and enhancing thermodynamic efficiency. It's worth noting that PEMs provided the greatest yield at 9.52 L/min and AWEs gained the highest efficiency of 61.74%.

*Corresponding author.

DOI: https://doi.org/10.51646/jsesd.v15i1.863

النمذجة الكيميائية الحرارية والكهروكيميائية باستخدام الماتلاب لتقييم أداء محللات التحليل الكهربائي للماء ذات درجة الحرارة المنخفضة

إبراهيم الطويل، زهرة جبريل، سالم معتوق، عبد الناصر صالح عامر، عبد الحميد سالم محمد العجمي

ملخص: تقدم هذه الدراسة نموذجاً حاسوبياً مبنياً على بيئة ماتلاب (MATLAB) للتحليل الكيميائي الحراري والكيميائي الكهربائي لتقنيات درجات الحرارة المنخفضة. يتنبأ النموذج بدقة بالحدود الديناميكية الحرارية ومؤشرات الأداء الرئيسية، بما في ذلك جهد الخلية العكوس وإنتاج الهيدروجين، كدالة لدرجة حرارة التشغيل. وتُظهر النتائج باستمرار أن ارتفاع درجة الحرارة يؤدي إلى تقليل الجهد العكوس للخلية والتغير في طاقة جيبس الحرة (G). ونتيجة لذلك، ينخفض استهلاك الطاقة الكهربائية اللازمة لشطر الماء، مما يُحسن من معدل إنتاج الهيدروجين. وقد أثبت هذا التحليل أن تشغيل المحلل الكهربائي عند درجات حرارة أعلى يؤدي بشكل مُطرد إلى أداءٍ أعلى في أنظمة غشاء التبادل الأنيوني (AEM) 50-80 درجة مئوية. والتحليل الكهربائي القلوي للماء (AWE) 60-90 درجة مئوية. وغشاء التبادل البروتوني (PEM) 50-100 درجة مئوية. وذلك من خلال خفض جهد الخلية، ومضاعفة كمية الهيدروجين المُنتجة في الدقيقة، وتعزيز الكفاءة الديناميكية الحرارية. وتجدر الإشارة إلى أن أنظمة PEM قد قدمت أعلى معدل إنتاج بلغ 9.52 لتر/دقيقة، في حين حققت أنظمة AWE الكفاءة الأعلى بنسبة 61.74%.

الكلمات المفتاحية: التحليل الكهربائي للماء، درجة حرارة تشغيل منخفضة، إنتاج الهيدروجين، كهروكيميائي، كيموحراري

1. INTRODUCTION

Water electrolysis is a promising method for converting and storing sustainable energy, especially for intermittent renewable sources. This process also produces high-purity hydrogen, which is essential for various industrial applications and to drive fuel cells. The core of low-temperature electrochemical water-splitting technologies such as alkaline, proton exchange membrane, and anion exchange membrane Electrolysers is based on two linked half-reactions: the hydrogen evolution reaction and the oxygen evolution reaction [1].

Hydrogen production through water electrolysis emerges as an environmentally friendly and sustainable method for chemical energy conversion, particularly effective for generating hydrogen when compared to alternative techniques. However, this widely recognized method for hydrogen production is characterized by its high cost and significant energy demands, which are typical for most industrial Electrolysers [2].

Electrolysis technologies are broadly categorized by their operating temperature and the type of ion-transporting electrolyte used. Alkaline (AWE), Proton Exchange Membrane (PEM), and Anion Exchange Membrane (AEM) electrolysis operate at temperatures between 50–80 °C. Among these, the low electrolysis is mature, commercially available, and widely utilized for hydrogen production [3].

Low-temperature electrolysis technologies play a vital role in facilitating clean hydrogen synthesis and the effective integration of renewable energy sources. AE is mature and uses low-cost catalysts but operates at lower current densities and pressures (~25-30 bar) [4].

This study clarifies the fundamental thermodynamic principles governing hydrogen production through electrolysis and its utilization in Electrolysers. It defines essential terminology (e.g., HHV, LHV, Gibbs Free Energy, Heat of Reaction/Formation) and outlines standard methods for efficiency calculation. Additionally, it compiles and summarizes information from various international case studies of wind-powered hydrogen production projects. It highlights that for electrolysis, the thermoneutral voltage (corresponding to the

enthalpy change, HHV for water splitting, ~1.48V) represents 100% thermal efficiency, whereas using the reversible voltage (~1.23V, corresponding to Gibbs Free Energy) leads to theoretical efficiencies >100% if external heat input isn't accounted for [5].

Electrolysis, though chemically straightforward, presents complexity in its energy demands for hydrogen production. The process, which involves splitting water, is non-spontaneous and requires a positive Gibbs free energy change (ΔG). Which equivalent to the inputs of an electrical energy, while the thermal energy component is given by $T \cdot \Delta S$, and the total energy input by ΔH. The enthalpy changes for hydrogen combustion (the reverse reaction) corresponds to hydrogen's lower heating value (LHV) of approximately 33.3 kWh/kg H2. Under standard conditions, liquid water electrolysis demands 32.7 kWh/kg H2 electrically, whereas steam electrolysis requires 31.5 kWh/kg H2 [3].

The different ٮlectrolyser types (e.g., PEM vs. SOEC) exhibit significantly different performance deviations under flexible operating modes compared to baseload, emphasizing the need for integrated, scenario-specific modeling to determine optimal siting, sizing, and operational strategies for minimizing hydrogen cost while maximizing asset value [6].

The classification of water electrolysis can be delineated based on the operational temperature regime, distinguishing between low-temperature electrolysis, characterized by functioning below 120°C, and high-temperature electrolysis [7].

Green hydrogen production is facilitated by coupling zero-emission electrochemical cycles with renewable energy infrastructures, such as wind-driven turbines [8], these advancements are essential for the technical evolution of water electrolysis and future power generation. By utilizing thermodynamic parameters and heat capacities, researchers have demonstrated how temperature-dependent variations influence the physical stability and transport efficiency of hydrogen-based systems. These insights, as presented by Bouzaid et al. (2025) [9], refine the interpretation of hole-based charge transfer and H+ transport by detailing the complex interplay between electronic states and host lattice distortions [9][10]

The aim of this study is analyzing and comparing the thermochemical and electrochemical performance of different Electrolyser types, specifically PEM and AWE according to varying of their operating temperatures. The study also visualizes key performance indicators such as voltages, gas production rates, power consumption, efficiencies, and changes in enthalpy and Gibbs free energy. The primary objective of this study to evaluate how thermodynamic and kinetic variations induced by temperature shifts affect the system-level energy efficiency of each electrolyser type within their typical operational ranges (spanning from 50°C to 100°C).

1.1. The Low Temperature Electrochemical Water Splitting

1.1.1. Alkaline Water Electrolysis (AWE)

Electrolysers typically utilize an aqueous potassium hydroxide (KOH) solution as the electrolyte. While other electrolyte options such as sulfuric acid (H_2SO_4), sodium chloride (NaCl), and sodium hydroxide (NaOH) are also utilized, a typical concentration range of 20 to 30 weight percent is maintained in the electrolyzing solution to optimize the equilibrium between the resistance of material corrosion and ionic conductivity. These Electrolysers demonstrate effective range of the operation temperature between 25 to 100 °C [11] [12].

The fundamental architecture of an alkaline electrolyser employs a unipolar configuration, featuring two metallic electrodes immersed within an aqueous electrolyte. Upon the application of an electrical current, the respective electrodes facilitate the generation of hydrogen and oxygen gases. This process enables the generation of hydrogen and oxygen gases. Figure 1 visually represents the operational principle of alkaline water electrolysis, while the associated electrochemical reactions are detailed in Equations (1) -(3) [13] [14], [15].

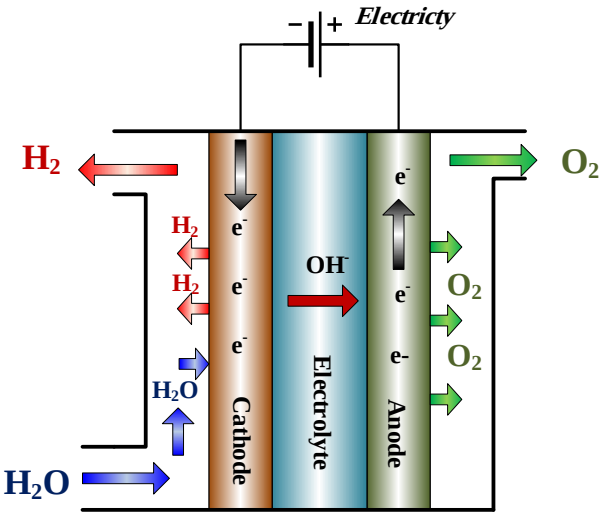

Figure 1. Alkaline electrolyser Cell.

The chemical equilibrium for an AWE system is outlined as follows:

The anode reaction involves: $$2OH^- \rightarrow H_2O + \frac{1}{2}O_2 + 2e^- \quad (1)$$

The cathode reaction is: $$2H_2O + 2e^- \rightarrow H_2 + 2OH^- \quad (2)$$

The overall reaction is: $$H_2O \rightarrow H_2 + \frac{1}{2}O_2 \quad (3)$$

1.1.2. The PEM Electrolysers (PEM)

Proton Exchange Membrane electrolyser (PEMEC) technology has drawn substantial academic interest due to its capability for efficient, high-purity hydrogen production, alongside its advantages in simplifying operational management and maintenance complexities [12]. PEMECs, operating at low temperatures (50-100°C). The water is supplied to the anode in PEMECs as shown in Figure (2), where it undergoes oxidation to produce oxygen and protons (H+). These protons then migrate across the proton-conducting membrane to the cathode, where they are reduced to form hydrogen gas [11].

The overall chemical balance can be deconstructed into two distinct half-reactions, each occurring at one of the electrodes [14], [15],[16]:

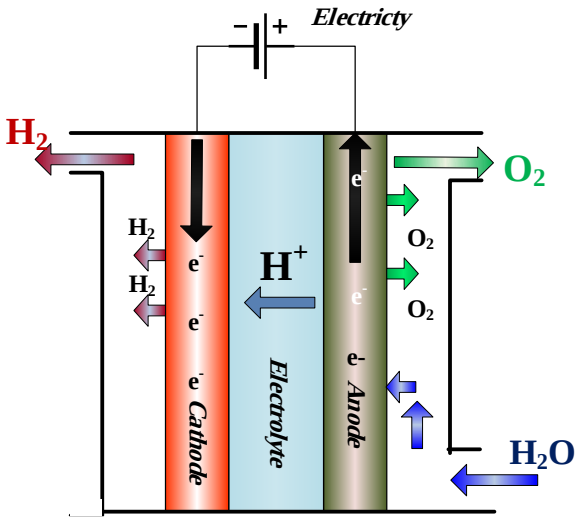

Figure 2. PEM Polymer Electrolyte Membrane.

The anode reaction proceeds as: $$H_2O \rightarrow 2H^+ + \frac{1}{2}O_2 + 2e^- \quad (4)$$

The cathode reaction is: $$2H^+ + 2e^- \rightarrow H_2 \quad (5)$$

The overall reaction: $$H_2O \rightarrow H_2 + \frac{1}{2}O_2 \quad (6)$$

1.1.3. The Anion Exchange Membrane Electrolyser (AEM)

The Anion Exchange Membrane Water Electrolyser (AEM) is a hybrid technology that combines the cost-effectiveness of traditional alkaline electrolysis with the high performance and compact design of proton-exchange membrane (PEM) Type.

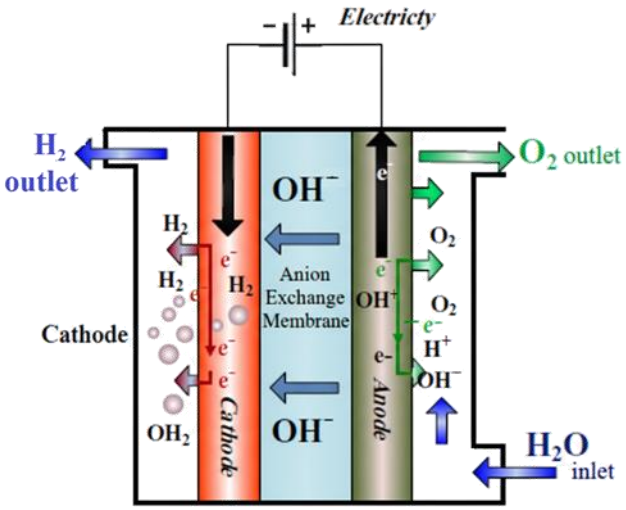

Figure 3. Anion Exchange Membrane electrolyser Cell.

In an AEM electrolyser, water is reduced at the cathode to produce hydrogen gas (H_2) and hydroxide ions (OH^-). The OH^- ions migrate through the anion exchange membrane to the anode, where they are oxidized to form oxygen gas (O_2) and release electrons. The electrons flow through the external circuit back to the cathode, while the membrane prevents gas mixing

and selectively transports OH^- ions, enabling efficient water splitting into hydrogen and oxygen [17], [18], [19].

The electrochemical reactions for water splitting in an alkaline AEM water Electrolyser cell [17], [18], [19]:

Anode Reaction: $2OH^- \rightarrow H_2O + \frac{1}{2}O_2 + 2e^-$ (7)

Cathode Reaction: $2H_2O + 2e^- \rightarrow H_2 + 2OH^-$ (8)

Overall Reaction: $H_2O \rightarrow H_2 + \frac{1}{2}O_2$ (9)

2. THE METHODOLOGY

This study employs a computational modeling approach using MATLAB to analyze and compare the thermochemical and electrochemical performance of low-temperature Polymer Electrolyte Membrane (PEM) and Alkaline Water Electrolysers (AWE). The methodology focuses on predicting thermodynamic limits, comparing Electrolyser technologies, and optimizing operating conditions for improved efficiency and hydrogen production.

2.1. Thermochemical and Electrochemical Analysis

2.2.1. Thermodynamics of Water Splitting

As an endergonic process, water electrolysis requires an external energy input due to its positive Gibbs free energy change ($\Delta G>0$), necessitates an external energy input to proceed. The thermodynamic feasibility and energy requirements of this reaction are quantitatively linked to electrical potential through the concepts of reversible voltage (Erev) and thermoneutral voltage (E_{tn}). These voltages provide a crucial connection between the thermodynamic properties of the electrochemical reaction and the electrical work required or produced by the system [12][16].

In an electrochemical cell, the cathode is denoted by a positive sign because electrons are consumed there, where a reduction reaction takes place, and electrons move into it. Conversely, the anode is denoted by a negative sign as electrons are liberated here, where an oxidation reaction occurs, and electrons move out of it.

2.2.2. Calculating Heat of Electrolyser Cell

The heat change associated with a reaction can be determined using the heats of formation of the compounds involved. The heat of formation is the energy change either released or absorbed, that occurs when a compound is formed from its basic elements:

$$\text{For the overall reaction, Heat} = \sum_{P} \text{heat}_f - \sum_{R} \text{heat}_f \quad (10)$$

Thermal energy is a fundamental consideration, from the pre-operational heating of Electrolysers and their continuous operational heat requirements, to the thermal transfer properties of components and the ultimate dissipation or utilization of waste heat [3].

From a thermodynamic perspective, applying the first law to the overall reactions results in:

$$\dot{Q}_j\text{-}\dot{W} = \left(\dot{n}\bar{h}\right)_P - \left(\dot{n}\bar{h}\right)_R \quad (11)$$

Where: $\dot{Q}_j$ is the generic rate of heat transfer kJ/kg, $\dot{W}$ is work, $\dot{n}_{H_2O}$= 1, $\dot{n}_{H_2}$= 1 and $\dot{n}_{O_2}$= ½ from half chemical reactions (3),(6), (9).

The electrical work per molar flow rate (Welec) is expressed as:

$$\bar{w}_{\text{elec}} = \bar{q}_{\text{EC}} - \left[\sum_P(\dot{n}\bar{h}) - \sum_R(\dot{n}\bar{h})\right] \quad (12)$$

Where, $\bar{q}_{\text{EC}}$ Heat per mole reacted (kJ/kmol)

A. The Entropy Balance

The equation below describes both the entropy balance of the chemical reaction and the overall heat transfer rate Q j at the system boundary's temperature Tj:

$$\frac{\text{dS}}{\text{dt}} = \frac{\dot{Q}_j}{T_j} + \sum_R(\dot{n}\bar{s}) - \sum_P(\dot{n}\bar{s}) + \dot{S}_{\text{gen}} \quad (13)$$

For steady-state conditions (ds/dt=0), the equation is reduced to:

$$\dot{Q}_j = T_j * \left[\sum_P(\dot{n}\bar{s}) - \sum_R(\dot{n}\bar{s}) - \dot{\text{S}}_{\text{gen}}\right] \quad (14)$$

An ideal Electrolyser operates as an internally reversible reaction. The generated heat, denoted as q_{FC}, is expelled from the system at a temperature T_{FC} and can be determined by:

$$\bar{q}_{EC} = T_{EC}.\bar{s}_{RP} \quad (15)$$

B. **Change in Gibbs energy (ΔG)**

The ΔG of the Electrolysers chemical process is a critical parameter for evaluating chemical energy transformations, particularly when pressure and volume variations are negligible. The initial step in quantifying the energy released from the reaction involves establishing a zero-reference point of energy for the constituent chemical elements, wherein the Gf of formation that defined as zero for the input state. Subsequently, the energy change ΔGf is determined by the change the products and the initial reactants [20], [21].

$$\Delta G_f = \Delta G_{f\ P} - \Delta G_{f\ R} \quad (16)$$

Where ΔG of a thermodynamic system is a function of both its enthalpy and entropy

$$G = H - T.S \quad (17)$$

The preceding equation, relating the enthalpy (H), system's temperature (T), and entropy (S), can be normalized on a per-mole basis for a given chemical species. This transformation yields the molar Gibbs free energy of formation as a function of the molar enthalpy of formation and the molar entropy [22], [23].

$$\Delta\bar{g}_{\text{f}} = [\Delta\bar{\text{h}}_{\text{f}} - (\text{T}.\Delta\bar{\text{s}})] \quad (18)$$

A. The Enthalpy of Overall Reaction

The standard change of enthalpy of formation $\Delta\bar{h}_f$ is calculated by subtracting the sum of the standard enthalpies of formation for the reactants $(\bar{h}_f)_R$ from the sum for the products $(\bar{h}_f)_P$. Similarly, the change of entropy $\Delta\bar{s}$ is the difference between the summed standard entropies of the products and the reactants. The enthalpy (h) and entropy (s) vary with temperature and pressure, requiring integration of molar heat capacity ($\bar{c}_p$) from the standard temperature (298.15 K) to determine values at non-standard conditions (hT). While standard values apply to stable forms $\bar{h}_{(T_o,P_o)}=\Delta\bar{h}^o_{f,298}=0$ and compounds $\bar{h}_{(T_o,P_o)}=\Delta\bar{h}^o_{f,298}$, adjusting for non-standard conditions is crucial for accurate thermodynamic calculations, as previously discussed [24], [25].

$$\bar{h}_{i(T,P)} = \left(\Delta\bar{h}^o_f\right)_{298,0.1MPa} + \left(\Delta\bar{h}\right)_{298,0.1MPa\ (T,P)} \quad (19)$$

$$\bar{h}_{298,0.1MPa\ (T,P)} = \left(\bar{h}_{(T,P)} - \bar{h}^o_{298}\right) \quad (20)$$

In Table 1, $\bar{h}_{298,0.1MPa\ (T,P)}$ signifies the difference between the enthalpy at a specific state and the reference enthalpy for an ideal gas at 0.1 MPa and 298.15 K [21][26].

Table (1) Properties of Ideal Gases at 25 °C and 100 kPa

c	$\bar{g}^o_f$	$\bar{s}^o_f$	$\bar{h}^o_f$
O_2	0	205.04	0
H_2	0	130.68	0
$H_2O(g)$	-228590	188.72	-241820
$H_2O(l)$	-237180	96.95	-285830

The molar enthalpy and molar entropy are dependent on temperature, described by the two equations below:

$$\bar{h}_{T,P} = \bar{h}^{\circ}_f + \int_{298}^{T} \bar{c}_p\, dT \quad (21)$$

$$\bar{s}_T = \bar{s}^{\circ}_{298} + \int_{298}^{T} \left(\frac{\bar{c}_p}{T}\right) dT \quad (22)$$

Additionally, the "molar heat capacity at constant pressure" (ēp kJ/kmol.K) is a function of temperature (T in K) and can be expressed as:

$$\bar{c}_p = a + bT + cT^2 + dT^3 \quad (23)$$

The constants (*a, b, c, and d*) are experimentally determined relevant to its properties are compiled in Table 2 [27] [26].

Table 2. Specific Heat at Constant Pressure for Ideal Gases

Gases	*a*	*b*	*c*	*d*
O_2	25.48	1.520×10^{-2}	-0.7155×10^{-5}	1.312×10^{-9}
H_2	29.11	-0.1916×10^{-2}	0.4003×10^{-5}	-0.8704×10^{-9}
H_2O	32.24	0.1923×10^{-2}	1.055×10^{-5}	-3.595×10^{-9}

The changes in molar enthalpy $\bar{h}_{T,P}$ and molar entropy $\bar{s}_T$ are directly determined from the molar enthalpy and molar entropy of the entire chemical reaction. The resulting values are then applied to equation (13) to find the change in molar Gibbs energy of formation $\Delta\bar{g}_f$ [23].

$$\Delta\bar{g}_f = (\bar{g}_f)_P - (\bar{g}_f)_R \quad (24)$$

B. Electric Work of the Electrolyser

The theoretical maximum electrical work achievable by an Electrolyser is quantitatively defined as the product of the negative of the number of moles of electrons transferred per mole of reactant (*n*), Faraday's constant (*F*), and the reversible cell potential (*E*), yielding a result in Joules.

$$\text{Electrical work done } W_{\text{electrical}} = \text{nFE} \quad (\text{J}) \quad (25)$$

Where the Faraday's constant is (96485.3 C/mol) [28].

This relationship, represents the thermodynamic upper bound of electrical energy that can be derived from the electrochemical reaction occurring within the Electrolyser under reversible operating conditions. For an Electrolyser operating under conditions of thermodynamic reversibility, the ΔG associated with the electrochemical reactions is equivalent to the electrical work input required by the system. Furthermore, this Gibbs free energy change is directly proportional to the thermodynamic decomposition voltage, which represents the theoretical minimum voltage necessary for the electrolysis reaction to occur under open-circuit conditions. [24]. Then:

$$w_{rev} = w_{max} = nFE = \Delta\bar{g}_f \quad (26)$$

The electromotive force (EMF) of an Electrolyser is its reversible open circuit voltage [20].

C. The Thermal Efficiency

The reversible efficiency of an Electrolyser (η_{rev}) is the quotient of the molar standard ($\Delta\bar{g}_f$) of formation, and the molar standard enthalpy of reaction ($\Delta\bar{h}_f$). This theoretical maximum efficiency is predicated on the assumption that all chemical species involved in the electrochemical reaction are maintained at their standard state conditions [22].

$$\eta_{rev} = \frac{\Delta\bar{g}_f}{\Delta\bar{h}_f} \times 100\% \quad (27)$$

2.2.3. Electrochemical of Water Splitting

A. The Reversible Potential

The reversible potential (E) is a direct measure of the change in Gibbs free energy (ΔG) during an electrochemical redox reaction. This relationship, which defines the thermodynamic force driving a reaction under specific conditions, is demonstrated by the Nernst equation, particularly when applied to the hydrogen reaction [29], [30]:

$$E = E^{o} + \frac{RT}{nF}\ln\left(\frac{P_{H_2}.P_{O_2}{}^{1/2}}{P_{H_2O}}\right) \quad (28)$$

R represents the universal gas constant (8.314 J/mol K) [25], and E° is the reversible standard potential of an electrochemical reaction [31], [32].

$$E^{o} = \frac{\Delta \bar{g}^{o}}{nF} \quad (29)$$

B. Cell Voltage Model

The actual operating voltage of an electrochemical cell V_{cell} is determined by the reversible thermodynamic potential and the different irreversible voltage losses (overpotentials) occurring during operation. Accordingly, the cell voltage can be expressed as [33] [34] [35] [36]:

$$V_{\text{cell}} = E_{\text{Nernst}} + \eta_{\text{act}} + \eta_{\text{ohm}} + \eta_{\text{conc}} \quad (30)$$

where E_{Nernst} represents the reversible equilibrium potential of the electrochemical reaction, while η_{act}, η_{ohm}, and η_{conc} denote the activation, ohmic, and concentration overpotential, respectively [34].

C. Activation Overpotential

The activation overpotential η_{act} arises from the electrochemical reaction kinetics at the electrode–electrolyte interface. In many electrochemical models, particularly under moderate current density conditions, the activation loss is approximated using a simplified Tafel expression [34]:

$$\eta_{\text{act}} = A_{\text{tafel}}\log_{10}(i) + B_{\text{tafel}} \quad (31)$$

where i is the current density. The Tafel coefficients are defined as [37]:

$$A_{\text{tafel}} = \frac{2.303RT}{\alpha nF}, \qquad B_{\text{tafel}} = -\frac{2.303RT}{\alpha F}$$

Where:

- R is the universal gas constant.
- T is the operating temperature,
- n is the number of electrons transferred in the electrochemical reaction.
- F is Faraday's constant,
- α is the charge transfer coefficient (typically in the range 0.3–0.7, commonly assumed to be around 0.5 in many studies) [38].

D. Ohmic Overpotential

The ohmic overpotential η_{ohm} accounts for resistive losses associated with ionic conduction through the electrolyte and electronic conduction through the electrodes and interconnects. It follows Ohm's law [33] [38]:

$$\eta_{\text{ohm}} = i\,r \quad (32)$$

where r is the total area-specific resistance (ASR) of the cell, which includes contributions from the electrolyte, electrodes, and contact resistances.

E. Concentration Overpotential (Mass Transport)

The concentration overpotential η_{conc}, also known as the mass transport overpotential, arises due to limitations in the transport of reactants to the reaction sites and removal of products from the electrodes. As the current density approaches the limiting current density i_{lim}, the concentration loss becomes significant and can be expressed as:

$$\eta_{\text{conc}} = -\frac{RT}{nF}\ln\left(1 - \frac{i}{i_{\text{lim}}}\right) \tag{33}$$

where i_{lim} represents the limiting current density determined by diffusion processes within the porous electrode structure and gas transport pathways.

F. Hydrogen Production Rate

The theoretical calculation of hydrogen production rates is based on the formulation presented below [41].

$$n_{H_2}(\text{mol/s}) = \frac{I_{\text{stack}}}{2F} \cdot n_{\text{cells}} \tag{34}$$

$$\text{Flow}_{\text{H}_2}\ (\text{L/min}) = \left(\frac{n_{H_2}(\text{mol/s}) \cdot R \cdot T}{P}\right) \cdot 60 \cdot 1000 \tag{35}$$

T denotes the Electrolysers operating temperature, *F* is the Faraday constant, p signifies the Electrolysers operating pressure, and *n* refers to the number of electron moles participating in the reaction [39].

G. Oxygen Production Rate:

$$n_{O_2}(\text{mol/s}) = \frac{n_{H_2}(\text{mol/s})}{2} \tag{36}$$

$$\text{Flow}_{\text{O}_2}\ (\text{L/min}) = \frac{\text{Flow}_{\text{H}_2}}{2} \tag{37}$$

H. Power Consumption:

The polarization curve in the stack can be expressed similarly like the product of the stack voltage V_{stack} with the stack current I_{stack} [42]:

$$P_{\text{electrical}} = V_{\text{cell}} \cdot I_{cell} \tag{38}$$

I. Thermoneutral Voltage (Etn):

The thermoneutral voltage represents the potential at which the electrical energy input precisely equals the enthalpy (ΔH) of the water-splitting reaction, facilitating an adiabatic operation.

$$E_{\text{tn}} = \frac{\Delta H}{nF} \tag{39}$$

This corresponds to the thermoneutral voltage, at which hydrogen and oxygen production reaches a thermal efficiency of 100% [43], [1].
Where F = 96,485 coulombs mole^{-1}, and n= 2 for hydrogen [42] [44].

J. Energy Efficiency

Energy efficiency functions as a primary metric for evaluating the performance of water Electrolyser cells and systems. When calculating this efficiency at the cell level, the evaluation focuses exclusively on the electrical energy input utilized for the electrolysis process, while disregarding other energy contributions, such as heat sources or auxiliary power consumption [1].

Energy efficiency is defined as the ratio of hydrogen energy outflow per unit time to the electrical power supplied. In the water electrolysis process, this efficiency is based on the electrical power provided for electrolysis, as expressed by the following equation [45]:

$$\eta_{\text{th}} = \frac{\Delta H \cdot n_{H_2}(\text{mol/s})}{P_{\text{electrical}}} \tag{40}$$

K. Voltage Efficiency:

Voltage Efficiency: In high-temperature scenarios, the calculation of the cell's voltage efficiency can be performed directly using the thermodynamic voltage [44].

$$\eta_{\text{voltage}} = \frac{E_{\text{rev}}}{V_{\text{cell}}} \tag{41}$$

L. Faraday Efficiency:

The faradaic efficiency, denoted as η_F, quantifies the efficacy of electron transfer within an electrochemical cell. This efficiency can be independently determined for each interface within the system. In the context of water electrolysis, a direct correlation exists between the applied current and the resulting gaseous chemical products [44].

$$\eta_F = 0.98 \tag{42}$$

M. Overall Efficiency:

$$\text{Efficiency}_{\text{overall}} = \text{Efficiency}_{\text{Faraday}} \cdot \text{Efficiency}_{\text{voltage}} \tag{43}$$

This relationship delineates the overall efficiency of Electrolysers. As the input current increases, the voltage efficiency (η_v) decreases while the Faraday efficiency (η_F) increases. At very low current densities and high differential pressure, the increase in η_F is greater than the decrease in η_v, leading to an improvement in electrical efficiency. While at ambient pressure, the decrease in ηv is more significant, and as a result, the overall efficiency is inversely proportional to the input current [44].

2.2.4. MATLAB Model Inputs

Table 3. contains the mechanical and electrical variables and constants used as inputs for the MATLAB model.

Table 3. inputs for the MATLAB model

Parameter	Value	Unit
Operating Pressure	1.01325×10^5	Pa
Current Density range	100 to 2000	A/cm^2
Active Area of the Cell	1	m^2
Number of Cells	1	-
Faraday's constant	96485	C/mol
Ideal Gas constant (R)	8.314	J/(mol · K)
Faradaic Efficiency	0.98	
Hydrogen's Higher Heating Value	286	(kJ/kmol H2)
Operating Temperature range	AEM (50-80C), AWE (60-90C), and PEM (50-100C)	°C

The flowchart of a MATLAB program developed to simulate the thermodynamic and electrochemical performance of the low Electrolysers type as shown in Appendix A1. Workspace preparation, calculation of initial physical, thermodynamic and electrolyser-based constants are carried out before the execution loop in which each type of electrolyser is assessed. The ranges for temperature and the values of the overpotential parameters for the selected electrolyser type are loaded, the values of total thermodynamic parameters (Molar Enthalpy, Entropy and Gibbs Free Energy) are calculated, as well as the Nernst and Thermoneutral voltages corresponding to this value of the overpotential parameter.

3. RESULTS AND DISCUSSION

Performance characteristic data Electrolysers were analyzed on temperature effect with thermodynamically and operation temperature is listed in Table A2 in Appendix A2.

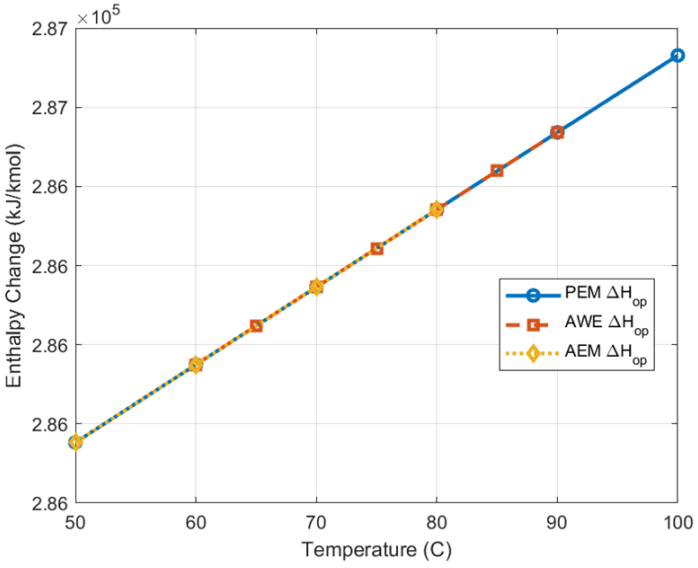

Figure 4. Enthalpy changes with operating temperature

Figure 4, represents the enthalpy change (ΔH) of the water-splitting reaction across a temperature range of 50°C to 100°C. The thermodynamic data shows an identical, linear increase for PEM, AWE, and AEM technologies, moving from approximately 2.86×10^5 kJ/kmol to 2.87×10^5 kJ/kmol. This uniform rise reflects the temperature dependence of the specific heat

capacities of liquid water, hydrogen, and oxygen gases. Because enthalpy represents the total thermal and electrical energy input required to break the molecular bonds of water, this upward trend confirms that a higher total energy input is required at elevated temperatures, an intrinsic thermodynamic characteristic independent of the electrolyser design.

Figure 5, displays the entropy change (ΔS) of the water electrolysis reaction across an operating temperature range of 50°C to 100°C. The entropy change exhibits an identical, linear upward trend for the PEM, AWE, and AEM Types, increasing from approximately 163.93 kJ/kmol·K to 165.34 kJ/kmol·K. This positive slope reflects the increasing molecular disorder and thermal energy storage capacity of the generated gases compared to the liquid water reactant as temperature rises. Because entropy is an intrinsic thermodynamic property of the chemical species involved, the results remain entirely uniform across all configurations, highlighting the fundamental thermodynamic baseline that dictates the thermal behavior of water-splitting systems.

Figure 6, depicts the Gibbs free energy change (ΔG_{op}) during water electrolysis as a function of operating temperature. All three electrolysers' configurations show an identical, linear reduction from 2.33×10^5 kJ/kmol at 50°C down to 2.25×10^5 kJ/kmol at 100°C. This steady decline is governed by the standard thermodynamic relationship $\Delta G = \Delta H - T \cdot \Delta S$, where the positive entropy change of the reaction causes the $T \cdot \Delta S$ term to grow larger at higher temperatures, thereby diminishing the Gibbs free energy requirement. This trend highlights the thermodynamic advantage of high-temperature operations, as it reduces the minimum electrical work required to drive the electrochemical decomposition of water.

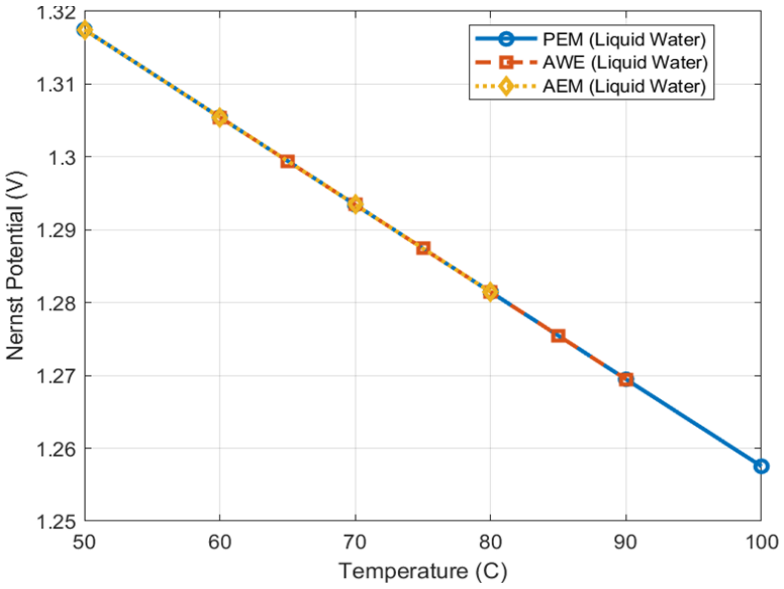

Figure 7: Nernst Potential vs. Operating Temperature

The Electrolysers shown in Figure. 7 characterize the Nernst potential with respect to temperature in Proton Exchange Membrane (PEM), Alkaline Water Electrolysis (AWE), and Anion Exchange Membrane (AEM) technologies. The linear, thermally induced, uniform decline in the reversible potential as a function of temperature in the three technologies occurs between 1.318 V (50°C) and 1.258 V (100°C). The decline is attributed to a reduction in the Gibbs free

energy for the water-splitting reaction. Since all three technologies employ liquid water as a reactant in the specified temperature range, the ideal, thermodynamic, reversible limits are the same. Thus, the open circuit voltage for electrolysis is lower in Electrolysers where the temperature is higher.

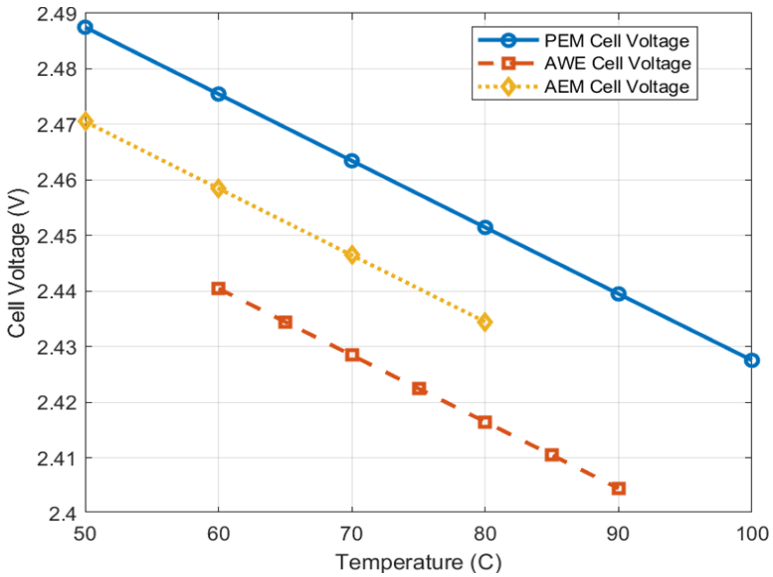

Figure 8. Cell Voltage vs. Operating Temperature

The AEM, PEM, and AWE Electrolysers show cell voltage behavior that is fundamentally different in the 50–100 °C range at constant current density, as shown in Figure. 8. Cell voltage decreases with temperature in all Electrolysers due to the reduction of activation and ohmic overpotential as charge transfer and ionic conductivity of the system's membranes and electrolytes are improved. The AWE system's operating cell voltage is the lowest of the three compared to the AEM and PEM Electrolysers, which reinforces a lower overpotential for the AWE system

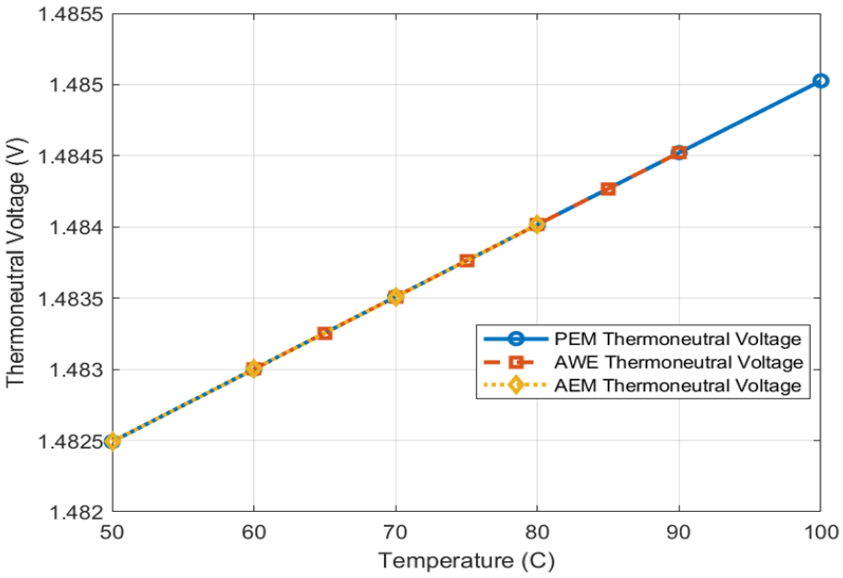

Figure 9: Thermoneutral Voltage vs. Operating Temperature

The AEM, PEM, and AWE Electrolysers show cell voltage behavior that is fundamentally different in the 50–100 °C range at constant current density, as shown in Figure. 8. Cell voltage

decreases with temperature in all Electrolysers due to the reduction of activation and ohmic overpotential as charge transfer and ionic conductivity of the system's membranes and electrolytes are improved. The AWE system's operating cell voltage is the lowest of the three compared to the AEM and PEM Electrolysers, which reinforces a lower overpotential for the AWE system.

Figure 9, illustrates thermoneutral voltages for PEM, AWE, and AEM Electrolysers as functions of operating temperature. These technologies display practically the same behavior, with all three technologies showing a minor linear increase from approximately 1.4825 V at 50°C to around 1.485 V at 100°C. This identical behavior occurs because the thermoneutral voltage is defined by the total enthalpy change of a water-splitting reaction; this is a state function of the chemical reactants and products, and not of the of the specific materials and transport phenomena of the various electrolyser cell types. The total energy requirement (the sum of the electrical work and the thermal energy) increases, to a small extent, as the temperature increases, when the system is allowed to operate in a perfectly insulated (i.e., adiabatic) state.

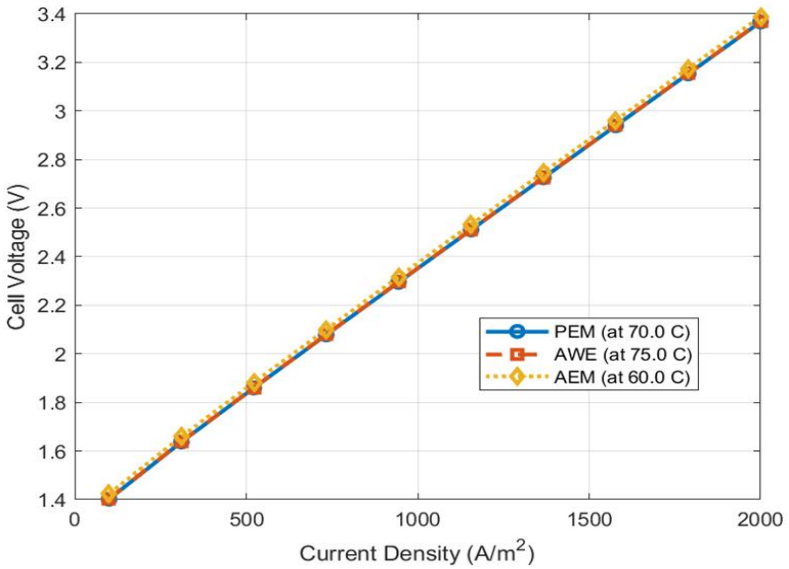

Figure 10: The electrolyzers Cell Voltage vs. Current Density

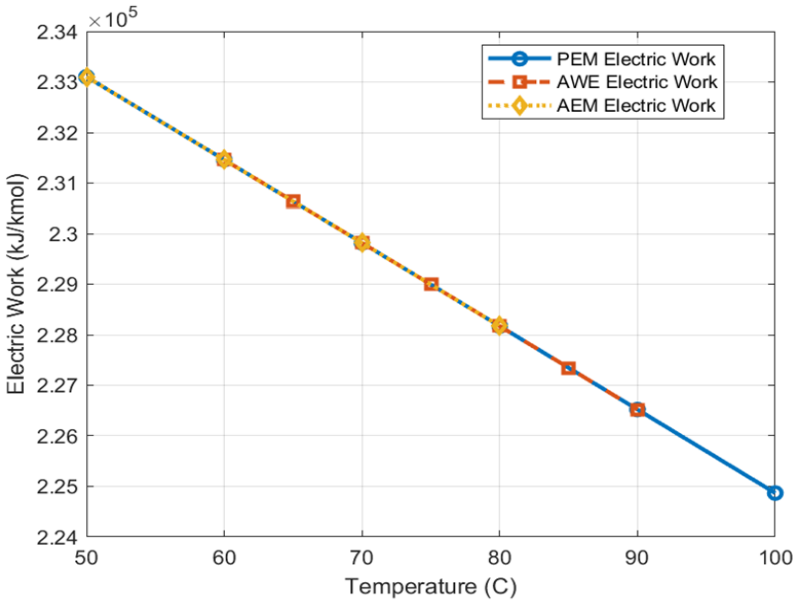

Figure 11. Electric Work vs. Operating Temperature

Figure 10, compares the polarization curves (cell voltage vs. current density) for a PEM electrolyser at 70°C, an AWE electrolyser at 75°C, and an AEM electrolyser at 60°C. All three profiles display a highly congruent, linear growth in cell voltage from around 1.4 V at 100 A/m² up to approximately 3.38 V at 2000 A/m². The slight divergence visible at higher current densities shows the AEM cell exhibiting marginally higher voltages, followed by the AWE cell, while the PEM cell maintains the lowest voltage profile at the upper current limit. This demonstrates that the superior proton conductivity of the PEM membrane at 70°C effectively counters ohmic losses at high current densities compared to its alkaline and anion-exchange counterparts.

Figure 11, traces the electrical work demand across a temperature span from 50°C to 100°C for PEM, AWE, and AEM Electrolysers. The curves for all three Electrolysers are completely congruent, decreasing linearly from 2.33×10^5 kJ/kmol to 2.25×10^5 kJ/kmol as temperature increases. This behavior directly parallels the Gibbs free energy trend, as the electrical work represents the non-expansion work required to drive a non-spontaneous electrochemical reaction under constant pressure and temperature conditions. The results signify that operating any of these liquid-water-fed Electrolysers at elevated temperatures systematically lowers the ideal electrical input threshold, which can significantly optimize overall system efficiency.

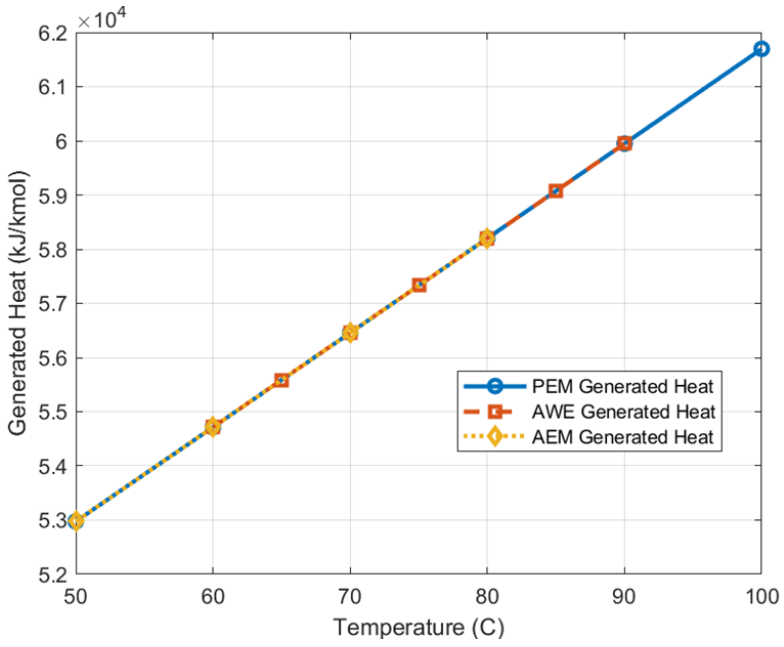

Figure 12. Generated Heat vs. Operating Temperature

Figure 12 illustrates the generated heat during operation across a temperature range of 50°C to 100°C for PEM, AWE, and AEM technologies. The figures show a uniform, identical linear increase for all three configurations, climbing from 5.3×10^4 kJ/kmol at 50°C to approximately 6.17×10^4 kJ/kmol at 100°C. This upward trend represents the entropic heat demand ($T \cdot \Delta S$) of the water-splitting process, which expands as the operating temperature rises. The perfectly overlapping profiles reinforce that the baseline thermal energy absorption required by the core chemical reaction depends solely on temperature variations rather than the distinct internal structural components of the membrane or alkaline Electrolysers.

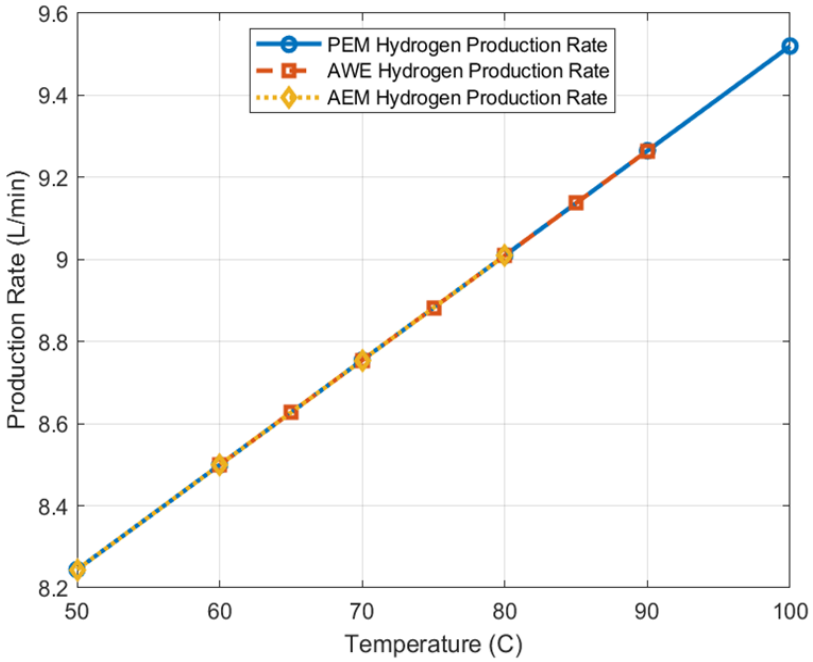

Figure 13. Hydrogen Production Rate versus Operating Temperature

Figure 13, shows the effect of temperature on the volumetric flow rate of hydrogen produced for a given current density. The results show a perfect, linear increase for each of the three electrolyser types, from approximately 8.24 L/min at 50°C to 9.52 L/min at 100°C. This uniform behavior is a consequence of Faraday's law of electrolysis, whereby the volumetric flow rate of the product is directly proportional to the current passing through the cell. The increase in the volumetric flow rate of the product gas is a result of a thermal increase in the gas, and shows that there is an effect of temperature of the volume of the output gas, with no effect on the various electrolyser cell architectures.

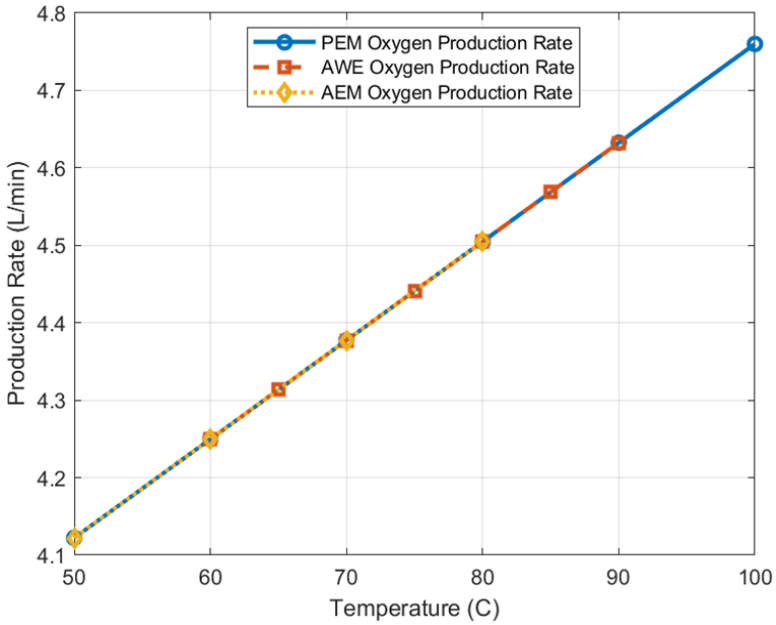

Figure 14. Oxygen Production Rate vs. Operating Temperature

Figure 14, presents the rate of oxygen generation as a function of temperature for the PEM, AWE, and AEM Electrolysers at a fixed current density. Similar to the hydrogen output, the rate of oxygen generation for all three Electrolysers rises in a linear fashion and identically from 4.12 L/min at 50 °C to 4.76 L/min at 100 °C. This identically linear behavior for all three Electrolysers is a result of the stoichiometry of the water-splitting reaction and Faraday's law, which states that the volume of oxygen generated will always be half of the volume of hydrogen produced. The line drawn by the point data shows an increase in volume from the gas, which indicates that the cell type and construction play no role in influencing faradaic conversion trends.

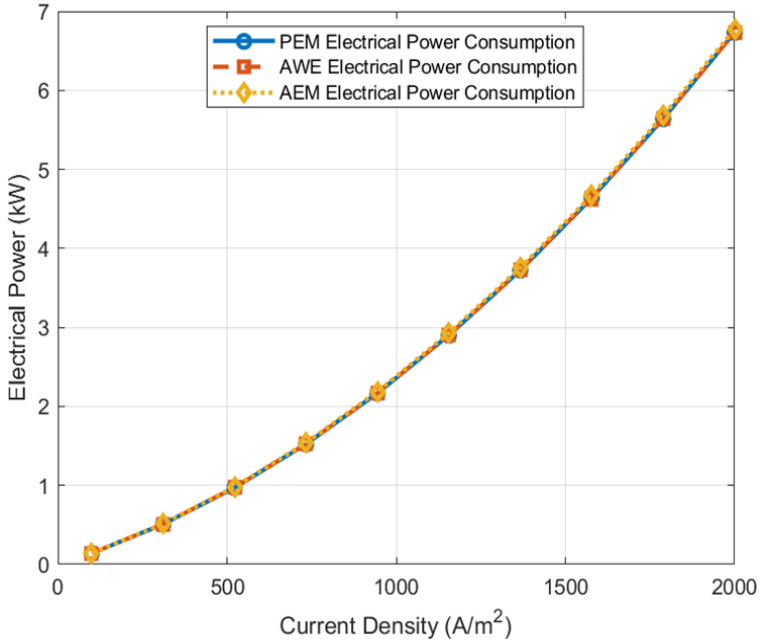

Figure 15. Electrical Power Consumption vs. Current Density

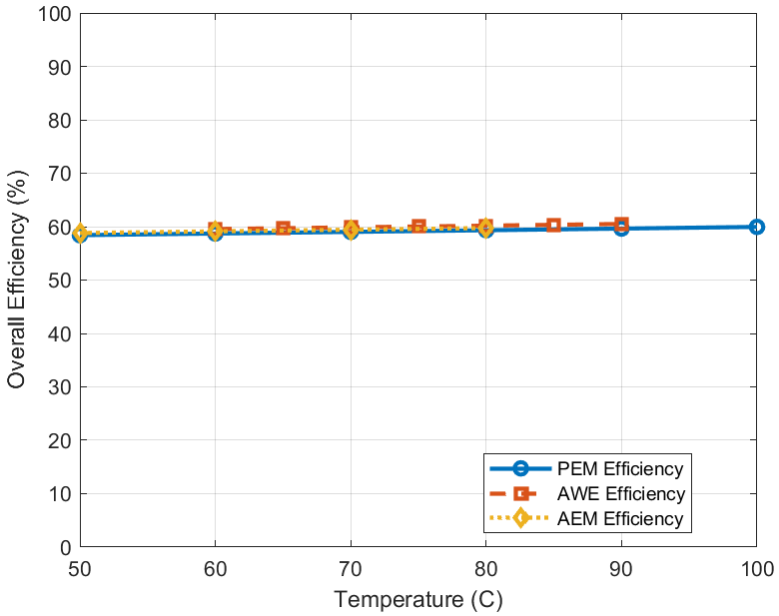

Figure 16: Energy Efficiency vs Operating Temperature

Figure 15 plots the relationship between the electrical consumption and current density for the PEM, AWE, and AEM Electrolysers. The cost increases identically and non-linearly in a parabolic shape for all three Electrolysers as the current density increases from 100 A/m² to 2000 A/m², and reaches an estimated value of 6.8 kW for all three Types. This identical behavior for all three Types is due to the combined effects of the activation and ohmic overpotentials at increased current density which leads to substantial voltage drop due to internal resistance. The curves for all three Types overlap completely at the current density values in question. Therefore, at the current density values in question, the main cost driver for all three Types is the same.

Figure 16, illustrates the variation of overall energy efficiency with operating temperature for three water electrolysis technologies: Anion Exchange Membrane (AEM), Alkaline Water Electrolyser (AWE), and Proton Exchange Membrane (PEM) Electrolysers. The results indicate that all three systems exhibit relatively stable energy efficiencies within the investigated temperature range of 50–100 °C, with efficiency values remaining close to 59–61%. This behavior suggests that temperature has only a minor influence on the overall energy conversion performance of the Electrolysers under the selected operating conditions.

4. CONCLUSIONS

This study of a thermochemical and electrochemical system illustrates how operating temperature and current density, as well as system performance are coupled at low operating temperature water electrolysis. As per the model results, high operating temperature reduces electric energy because of reduced reversible voltage and Gibbs free energy change and results in increased hydrogen and oxygen production rates. Although the high temperature requires a higher amount of thermal input to ensure the system thermoneutrality the electric energy consumed is lower so that the performance is improved and Alkaline water Electrolysers are affected significantly by high temperature in efficiency improvement due to improvement of ionic conductivity and lower overpotentials, compared to Anion Exchange Membrane Electrolysers that are less affected by high temperatures. The PEM Electrolyser presents higher hydrogen generation rate at high temperature (9.52 L/min) whereas the AWE shows better efficiency (61.74 %).

Author Contributions: The significant contributions of all authors to this work are delineated according to the following task distribution:

a) Ibrahim H. Tawil: Conceptualization, methodology, programming, writing the original draft, writing an introduction, writing the explanation of results, publishing.
b) Zahra Gebrel: Conceptualization, methodology, supervision, publishing.
c) Salem Matouq Khamkhem: Contributed to conceptualization, methodology development, drafting the initial manuscript, conducting the literature review, formulating the explanation of results, and managing publication.
d) Abdulnasir. S. Amir: Writing the original draft, writing an introduction, writing the explanation of results, publishing.
e) Abdulhamid Salim Alajmi: Writing a literature review, writing the explanation of results, publishing.

Financial Support: This research did not receive any dedicated funding from public, private, or non-profit sources.

Data Availability Statement: The data from this study can be obtained by contacting the corresponding author.

Conflicts of Interest: No conflicts of interest were reported by the authors.

Using the Artificial intelligence: It was used to assist with translation, rephrasing some sentences, and helping to debug programming errors.

Acknowledgments: The authors express their gratitude to those responsible for the joint doctoral project in the Western Region, Faculty of Science, University of Tripoli, for their constant support.

APPENDIXIES

Appendix A1: The flowchart of a MATLAB code

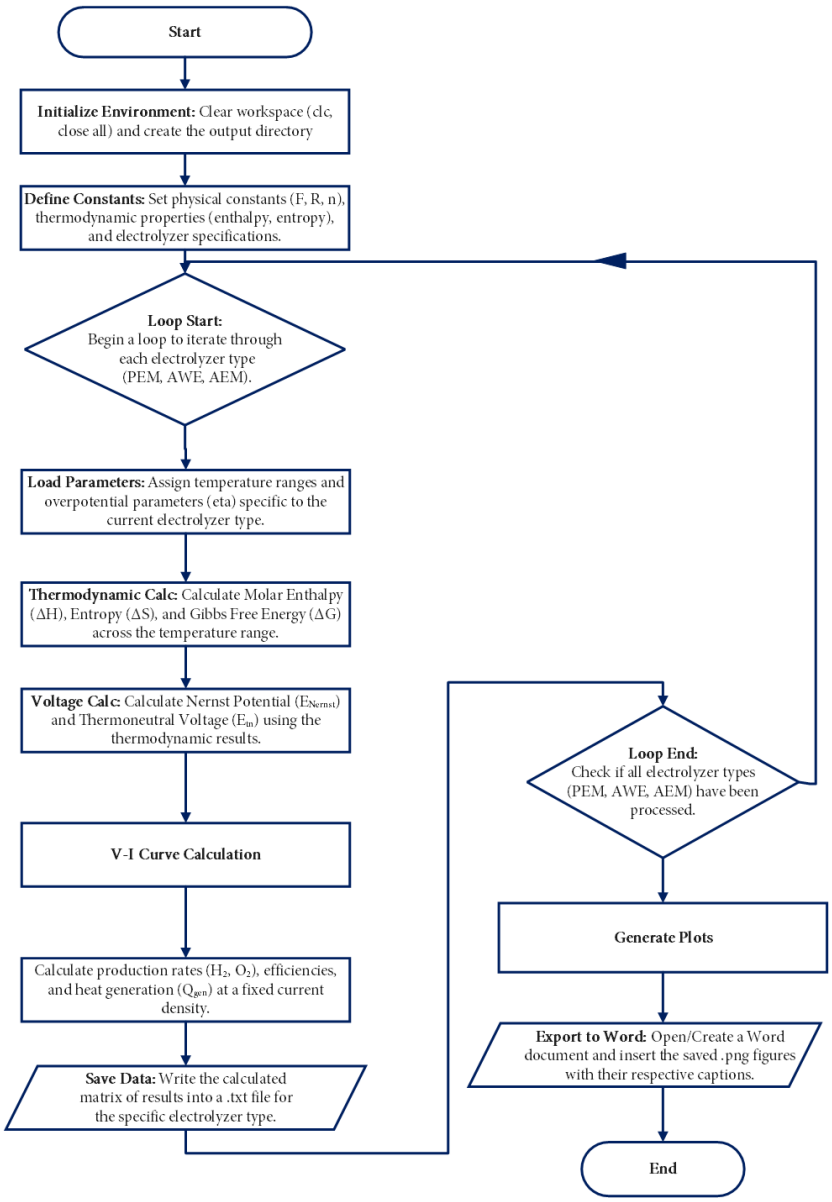

Figure A1. the flowchart of a MATLAB code

Appendix A2: Table A2: Comparison of AEM, AWE, and PEM Electrolyser Parameters

Table A2: Comparison of AEM, AWE, and PEM Electrolyser Parameters

	AEM		AWE		PEM	
Operating Temperature (C)	Min	Max	Min	Max	Min	Max
	50	80	60	90	50	100
Reversible Voltage (V)	1.3175	1.2815	1.3055	1.2695	1.3175	1.2575
Cell Voltage (V)	2.4705	2.4345	2.4405	2.4045	2.4875	2.4275
Thermoneutral Voltage (V)	1.4825	1.484	1.483	1.4845	1.4825	1.485
Nernst Voltage (V)	1.3175	1.2815	1.3055	1.2695	1.3175	1.2575
H_2 Production (L/min)	8.24	9.01	8.50	9.26	8.24	9.52
O_2 Production (L/min)	4.12	4.50	4.25	4.63	4.12	4.76
P_{elec} (kW)	2470.49	2434.45	2440.46	2404.48	2487.49	2427.52
η_{th} (%)	60.01	60.96	60.77	61.74	59.60	61.17
ΔH (kJ/kmol)	286076.5	286370.6	286174.8	286468.2	286076.5	286565.4
W_{ele} (kJ/kmol)	476.73	469.78	470.94	463.99	480.01	468.44
Q_{gen} (kJ/kmol)	-285599.8	-285900.9	-285703.9	-286004.2	-285596.5	-286097.0
ΔG (kJ/kmol)	233101.2	228169.9	231460.3	226520.5	233101.2	224868.4
ΔS (kJ/kmol.K)	163.93	164.80	164.23	165.08	163.93	165.34

Appendix A3: Thermodynamic and Electrochemical Symbols

Symbol	Definition
α	Charge transfer coefficient
A_{tafel}, B_{tafel}	Tafel coefficients used to calculate activation overpotential
a, b, c, d	Experimentally determined constants for calculating specific heat at constant pressure
c_p / $\overline{c}_p$	Specific / molar heat capacity at constant pressure
E / E_{rev}	Reversible cell potential / Reversible voltage
E°	Reversible standard potential of an electrochemical reaction
E_{Nernst}	Reversible equilibrium potential (Nernst potential)
E_{tn}	Thermoneutral voltage
η_{act}	Activation overpotential
η_{conc} / $\eta_{mass\ transport}$	Concentration overpotential / Mass transport overpotential
η_F	Faradaic efficiency
η_{ohm} / η_{ohmic}	Ohmic overpotential
η_{rev}	Reversible efficiency of an Electrolyser
η_{th}	Thermal efficiency / Energy efficiency
$\eta_{voltage}$ / η_v	Voltage efficiency
F	Faraday's constant
ΔG / G	Change in Gibbs free energy / Gibbs free energy
ΔG_f / Δg_f	Total/molar change in Gibbs free energy of formation

ΔH / H	Total enthalpy change / Enthalpy
Δh_f	Standard change of enthalpy of formation
I_{cell} / I_{stack}	Cell current / Stack current
i / i_{lim}	Current density / Limiting current density
N_{cells} / n_{cells}	Number of cells in a stack
n	Number of electrons transferred per mole of reactant
n_{H2O}, n_{H2}, n_{O2}	Number of moles of water, hydrogen, and oxygen
P	Operating pressure
P_{elec}	Electrical power consumption
P_{H2}, P_{O2}, P_{H2O}	Partial pressures of hydrogen, oxygen, and water
Q_j	Generic rate of heat transfer
q_{EC}	Heat per mole reacted / Generated heat
R	Universal gas constant
r	specific resistance of the cell
ΔS / S	Total entropy change / Entropy
Δs	Change of entropy
S_{gen}	Entropy generation
T	Temperature
V_{cell}	Cell voltage
V_{stack}	Stack voltage
W / w_{elec}	Work / Electrical work
w_{rev} / w_{max}	Reversible maximum electrical work

REFERENCES

[1] *W. Li, H. Tian, L. Ma, Y. Wang, X. Liu, and X. Gao, "Low-temperature water electrolysis: fundamentals, progress, and new strategies," Mater. Adv., vol. 3, no. 14, pp. 5598–5644, 2022, doi: 10.1039/d2ma00185c.*

[2] *M. E. Şahin, "An Overview of Different Water Electrolyser Types for Hydrogen Production," Energies (Basel)., vol. 17, no. 19, p. 4944, Oct. 2024, doi: 10.3390/en17194944.*

[3] *A. Franco and C. Giovannini, "Recent and Future Advances in Water Electrolysis for Green Hydrogen Generation: Critical Analysis and Perspectives," Sustainability (Switzerland), vol. 15, no. 24, 2023, doi: 10.3390/su152416917.*

[4] *A. Pozio, F. Bozza, G. Nigliaccio, M. Platter, and G. Monteleone, "Development perspectives on low-temperature electrolysis," Energia, ambiente e innovazione, vol. 1, pp. 66–71, 2021, doi: 10.12910/EAI2021-014.*

[5] *K. W. Harrison, Remick R., G. D. Martin, and A. Hoskin, "Hydrogen Production: Fundamentals and Case Study Summaries," Hydrogen and fuel cells, no. January, pp. 207–226, 2010.*

[6] *A. Chandrasekar and B. Westlake, "MODELING THE FLEXIBLE OPERATION OF ELECTROLYSERS FOR HYDROGEN PRODUCTION IN A LOW-CARBON ENERGY SYSTEM Important Considerations," no. August, pp. 0–9, 2022, [Online]. Available: https://us-regen-docs.epri.com.*

[7] *L. Jin, R. N. Nakashima, G. Comodi, and H. L. Frandsen, "Alkaline electrolysis for green hydrogen production: techno-economic analysis of temperature influence and*

control," 36th International Conference on Efficiency, Cost, Optimization, Simulation and Environmental Impact of Energy Systems, ECOS 2023, pp. 908–919, 2023, doi: 10.52202/069564-0082.

[8] C. Laghlimi, A. Moutcine, Y. Ziat, A. Koufi, S. Bouyassan, and H. Belkhanchi, "Hydrogen: chronology and electrochemical production Charaf," Solar Energy and Sustainable Development, vol. 0, no. The 2024 1st International Conference on Materials Sciences and Mechatronics for Sustainable Energy and the Environment, pp. 22–37, 2024, doi: https://doi.org/10.51646/10.51646/jsesd.v14iSI_MSMS2E.405.

[9] A. Bouzaid, Y. Ziat, H. Belkhanchi, and H. Fatihi, "Boosting the photocatalytic hydrogen production via the S/Zr co-doping in a CaTiO3 perovskite: first-principles study of the optoelectronic, thermodynamic, and photocatalytic," European Physical Journal B, vol. 98, no. 7, 2025, doi: 10.1140/epjb/s10051-025-01004-2.

[10] A. Bouzaid, Y. Ziat, and H. Belkhanchi, "Prediction the effect of (S, Se, Te) doped MgTiO3 on optoelectronic, catalytic, and pH conduct as promised candidate photovoltaic device: Ab initio framework," Int. J. Hydrogen Energy, vol. 100, pp. 20–32, Jan. 2025, doi: 10.1016/j.ijhydene.2024.12.284.

[11] and A. E. Rakesh Krishnamoorthy lyer, Jarod C. Kelly, "Electrolysers for Hydrogen Production: Solid Oxide, Alkaline, and Proton Exchange Membrane," 2022.

[12] M. El-Shafie, "Hydrogen production by water electrolysis technologies: A review," Results in Engineering, vol. 20, Dec. 2023, doi: 10.1016/j.rineng.2023.101426.

[13] F. Gambou, D. Guilbert, M. Zasadzinski, and H. Rafaralahy, "A Comprehensive Survey of Alkaline Electrolyser Modeling: Electrical Domain and Specific Electrolyte Conductivity," Energies (Basel)., vol. 15, no. 9, p. 3452, May 2022, doi: 10.3390/en15093452.

[14] M. Nasser, T. F. Megahed, S. Ookawara, and H. Hassan, "A review of water electrolysis–based systems for hydrogen production using hybrid/solar/wind energy systems," Environmental Science and Pollution Research, vol. 29, no. 58, pp. 86994–87018, Dec. 2022, doi: 10.1007/s11356-022-23323-y.

[15] N. Gallandat, K. Romanowicz, and A. Züttel, "An Analytical Model for the Electrolyser Performance Derived from Materials Parameters," Journal of Power and Energy Engineering, vol. 05, no. 10, pp. 34–49, 2017, doi: 10.4236/jpee.2017.510003.

[16] M. Pfennig, B. Schiffer, and T. Clees, "Thermodynamical and electrochemical model of a PEM Electrolyser plant in the megawatt range with a literature analysis of the fitting parameters," Int. J. Hydrogen Energy, Feb. 2024, doi: 10.1016/j.ijhydene.2024.04.335.

[17] H. W. J. Sol A Lee, Jaehyun Kim, Ki Chang Kwon, Sun Hwa Park, "Anion exchange membrane water electrolysis for sustainable large-scale hydrogen production," Carbon Neutralization -WILEY, vol. 1, no. 1, pp. 26–48, 2022, doi: 10.1002/cnl2.9.

[18] A. Hasan, V. Prasad, S. Afghan, F. Khalid, M. Hanafi, and B. Azami, "International Journal of Hydrogen Energy Mathematical modelling of a photoelectrochemical anion exchange membrane electrolyser for sustainable hydrogen production," Int. J. Hydrogen Energy, vol. 140, no. November 2024, pp. 1233–1240, 2025, doi: 10.1016/j.ijhydene.2024.11.415.

[19] Z. Fang et al., "Review Stability challenges of anion-exchange membrane water Electrolysers from components to integration level," Chem Catalysis, vol. 4, no. 10, p. 101145, 2024, doi: 10.1016/j.checat.2024.101145.

[20] A. L. Dicks and D. A. J. Rand, Fuel cell systems explained, 3rd ed. John Wiley & Sons, 2018. doi: 10.1002/9781118706992.

[21] C. Borgnakke and R. E. Sonntag, Fundamentals of thermodynamics. John Wiley & Sons, 2020.

[22] N. Srivastava, "Modeling of solid oxide fuel cell/gas turbine hybrid systems," 2006.

[23] T. M. Koehler, D. B. Jarrell, and L. J. Bond, "High Temperture Ceramic Fuel Cell Measurement and Diagnostics for Application to Solid Oxide Fuel Cell Systems," Office of Scientific and Technical Information ({OSTI}), 2001. doi: 10.2172/965697.

[24] K. Annamalai, I. K. Puri, and M. A. Jog, Advanced Thermodynamics Engineering. 2011. doi: 10.1201/9781439805718.

[25] W. Winkler, Thermodynamics. Elsevier, 2016. doi: 10.1016/B978-0-12-410453-2.00003-8.

[26] M. K. ÇENGEL, YUNUS A, MICHAEL A. BOLES, THERMODYNAMICS: AN ENGINEERING APPROACH, NINTH EDITION. 2016.

[27] C. BORGNAKKE and R. E. SONNTAG, FUNDAMENTALS OF THERMODYNAMICS, 7th ed. 2009.

[28] NETL, "Seventh Edition Fuel Cell Handbook," Pittsburgh, PA, and Morgantown, WV, 2004. doi: 10.2172/834188.

[29] I. H. Tawil, F. M. Bsebsu, and H. Abdulkader, "Thermodynamic Study of Operation Properties Effect on Polymer Electrolyte Membrane Fuel Cells (PEM)," Solar Energy and Sustainable Development journal, vol. 7, no. 1, Feb. 2021, doi: 10.51646/jsesd.v7i1.67.

[30] T.-I. Tsai, "Carbon Formation in Solid Oxide Fuel Cells During Internal Reforming and Anode Off-Gas Recirculation," The University of Birmingham.

[31] K. M. J. Andersson, "Solid Oxide Fuel Cell Modeling at the Cell Scale," Lund University. doi: 10.13140/RG.2.2.12858.59846.

[32] S. R. Pakalapati and I. Celik, "A new reduced order model for solid oxide fuel cells," West Virginia University Libraries, 2006. doi: 10.33915/etd.3458.

[33] S. Yosaf, H. Gnaifaid, and A. Mizda, "Thermoeconomic Assessments of Green Hydrogen Production Via PV&PEM Electrolyser:," Solar Energy and Sustainable Development Journal, vol. 13, no. 1, pp. 57–70, Mar. 2024, doi: 10.51646/jsesd.v13i1.172.

[34] H. Ahmed and A. Musa, "Performance Investigation of Direct oupling Advanced Alkaline Electrolysis and PEMFC System," Solar Energy and Sustainable Development journal, vol. 9, no. 2, 2021, doi: 10.51646/jsesd.v9i2.7.

[35] J. Wang, J. Wen, J. Wang, B. Yang, and L. Jiang, "Water Electrolyser operation scheduling for green hydrogen production: A review," Renewable and Sustainable Energy Reviews, vol. 203, 2024, doi: 10.1016/j.rser.2024.114779.

[36] M. PINO KIRSCH, Nilsson, "Electrolyser Performance and Degradation under Various Load Shapes," KTM, 2024.

[37] M. Carmo, D. L. Fritz, J. Mergel, and D. Stolten, "A comprehensive review on PEM water electrolysis," Int. J. Hydrogen Energy, vol. 38, no. 12, pp. 4901–4934, 2013, doi: 10.1016/j.ijhydene.2013.01.151.

[38] H. A. Khater, A. A. Abdelraouf, and M. H. Beshr, "Optimum Alkaline Electrolyser-Proton Exchange Membrane Fuel Cell Coupling in a Residential Solar Stand-Alone Power System," ISRN Renewable Energy, vol. 2011, pp. 1–13, 2011, doi: 10.5402/2011/953434.

[39] Á. Hernández-Gómez, V. Ramirez, D. Guilbert, and C. Consumption´angel Hernández-Gómez, "Investigation of PEM Electrolyser modeling: Electrical domain, efficiency, and specific energy consumption Investigation of PEM Electrolyser model-ing: Electrical domain, efficiency, and specific energy consumption Investigation of PEM Electrolyser modeli," Int. J. Hydrogen Energy, 2020, doi: 10.1016/j.ijhydene.2020.03.195ï.

[40] F. Calise, F. L. Cappiello, L. Cimmino, M. D. D'accadia, and M. Vicidomini, "Dynamic simulation and thermoeconomic analysis of a hybrid renewable system based on PV and

fuel cell coupled with hydrogen storage," Energies (Basel)., vol. 14, no. 22, 2021, doi: 10.3390/en14227657.

[41] H. F. Araújo, J. A. Gómez, and D. M. F. Santos, "Proton-Exchange Membrane Electrolysis for Green Hydrogen Production: Fundamentals, Cost Breakdown, and Strategies to Minimize Platinum-Group Metal Content in Hydrogen Evolution Reaction Electrocatalysts," Catalysts, vol. 14, no. 12, 2024, doi: 10.3390/catal14120845.

[42] H. L. Lord, W. Zhan, and J. Pawliszyn, "Fundamentals and Applications of Needle Trap Devices," in Comprehensive Sampling and Sample Preparation, Elsevier, 2012, pp. 677–697. doi: 10.1016/B978-0-12-381373-2.00056-9.

[43] H. Sayed-Ahmed, I. Toldy, and A. Santasalo-Aarnio, "Dynamic operation of proton exchange membrane Electrolysers—Critical review," Renewable and Sustainable Energy Reviews, vol. 189, no. PA, p. 113883, 2024, doi: 10.1016/j.rser.2023.113883.

[44] Á. Hernández-Gómez, V. Ramirez, and D. Guilbert, "Investigation of PEM Electrolyser modeling: Electrical domain, efficiency, and specific energy consumption," Int. J. Hydrogen Energy, vol. 45, no. 29, pp. 14625–14639, 2020, doi: 10.1016/j.ijhydene.2020.03.195.

[45] M. Khaleel et al., "Towards Hydrogen Sector Investments for Achieving Sustainable Electricity Generation," Solar Energy and Sustainable Development, vol. 13, no. 1, pp. 71–96, 2024, doi: 10.51646/jsesd.v13i1.173.

[46] K. W. Harrison, Remick R., G. D. Martin, and A. Hoskin, "Hydrogen Production: Fundamentals and Case Study Summaries," Hydrogen and fuel cells, no. January, pp. 207–226, 2010.

[47] M. M. Rashid, M. K. Al Mesfer, H. Naseem, and M. Danish, "Hydrogen Production by Water Electrolysis: A Review of Alkaline Water Electrolysis, PEM Water Electrolysis and High Temperature Water Electrolysis," Int. J. Eng. Adv. Technol., vol. 8958, no. 3, pp. 2249–8958, 2015.